Journal of Orthopaedic Translation 38 (2023) 203–212

Contents lists available at ScienceDirect

Journal of Orthopaedic Translation

journal homepage: www.journals.elsevier.com/journal-of-orthopaedic-translation

original article

Combination of cobalt, chromium and titanium nanoparticles increases cytotoxicity *in vitro* and pro-inflammatory cytokines *in vivo*

Zhao Liu [a,h], Hui Liu [b,1], Rachel Vowden [c], Louise Hughes [d], Dahu Qi [e], Wendy Francis [f], Giorgio Perino [g], Ryan Pink [c], Jun Xiao [e], Bin Li [a], Zhidao Xia [f,*]

[a] *Department of Orthopedic Surgery, Orthopedic Institute, The First Affiliated Hospital, Suzhou Medical College, Soochow University, Suzhou, Jiangsu, China*
[b] *Department of Orthopedics Trauma and Microsurgery, Zhongnan Hospital of Wuhan University, Wuhan, China*
[c] *Department of Biological and Medical Sciences, Faculty of Health and Life Sciences, Oxford Brookes University, Oxford, UK*
[d] *Oxford Instruments NanoAnalysis, Halifax Road, High Wycombe, Bucks, UK*
[e] *Department of Orthopedic Surgery, Tongji Hospital, Tongji Medical College, Huazhong University of Science and Technology, Wuhan, China*
[f] *Centre for Nanohealth, Swansea University Medical School, Singleton Park, Swansea, UK*
[g] *Department of Orthopedics and Orthopedic Surgery, University Medicine Greifswald, Greifswald, Germany*
[h] *State Key Laboratory of Molecular Engineering of Polymers, Fudan University, Shanghai, China*

ARTICLE INFO

Keywords:
Metal nanoparticles
Macrophages
Cytotoxicity
Pro-inflammatory cytokines

ABSTRACT

Background: The mixture of different metallic nanoparticles released from intended and unintended wearing of orthopaedic implants such as the Co/Cr cup and head, Co/Cr sleeves or tapers and their interface with Ti stems in the case of hip prostheses are a leading cause of adverse inflammatory responses and cytotoxicity to the host.
Methods: This study assessed the *in vitro* cytotoxic effects of three metallic nanoparticles (Co, Cr and Ti) separately and in combination on macrophages. The *in vivo* effects were also evaluated after peri-tibial soft tissue injection in mice.
Results: The results demonstrated that Co, Cr, and Ti nanoparticles and their combination were phagocytosed by macrophages both *in vitro* and *in vivo*. High doses of nanoparticles from each individual metal caused a variable rate of cell death *in vitro*. However, the mixture of Co/Cr/Ti nanoparticles was more toxic than the Co, Cr or Ti metals alone at low doses. Intracellular distribution of Co, Cr, and Ti in the combined group was heterogeneous and associated with distinct morphological features. The results from *in vivo* experiments showed a significant increase in the mRNA levels of interleukin (IL)-1β, IL-6, IL-8 and tumour necrosis factor (TNF)-α in peri-tibial soft tissue following the administration of Co alone as well as the combination of nanoparticles.
Conclusion: This study demonstrated that the combination of Co/Cr/Ti nanoparticles was more cytotoxic than any of the individual metals *in vitro* and induced higher expression of genes encoding pro-inflammatory cytokines than single metals *in vivo*. The *in vivo* model utilised in this study might provide a useful tool for rapid assessment of the effects of unintended release of metal nanoparticles from implants in pre-/post-marketing studies.
Translational potential of this article: This study highlights the importance of preclinical assessments of potential nanoparticles produced by wear and tear of metal implants using macrophages and animal models, in particular their combinational toxicity in addition to the assessments of the bulk metallic materials.

1. Introduction

Metal alloys are widely used in arthroplasty of major joints [1–7], expanding also to smaller joints [8] and have found a new application in the additive manufacturing of customised implants [9].

Orthopaedic implants generate wear particles by different mechanisms, which can be divided into two main groups: a) mechanical, comprising abrasion, erosion, adhesion, and surface fatigue; b) mechanical with an additional element of active chemistry, oxidation and/or corrosion [10]. Wear particles originate from the contact surfaces of the implants, which consist of the bearing surface and junctions of the various components.

* Corresponding author. Centre for Nanohealth, Swansea University Medical School, Singleton Park, Swansea, SA2 8PP, UK.
E-mail address: z.xia@swansea.ac.uk (Z. Xia).
[1] Equal contribution as the first author

https://doi.org/10.1016/j.jot.2022.10.013
Received 22 May 2022; Received in revised form 6 October 2022; Accepted 20 October 2022

In second-generation metal-on-metal (MoM) hip implants, metal nanoparticles are generated at the bearing surface of the cobalt-chrome-molybdenum alloy (CoCrMo) after MoM hip resurfacing arthroplasty (HRA) by tribocorrosion (intended wear) and/or edge loading (unintended wear) [11] and at the titanium (Ti) neck taper junction after CoCrMo MoM large head (LH) total hip arthroplasty (THA), with or without a CoCrMo metallic adapter sleeve (MAS) [12,13]. In non-MoM THA implants, metal corrosion occurs at the CoCrMo dual modular neck (DMN) junction with the Ti alloy stem [14].

Previous study of clinical samples has shown that the combination of Co, Cr and Ti metal nanoparticles resulted in more severe clinical complications than Co/Cr nanoparticles. However, the underlying mechanism is unclear [15].

Wear particles are also generated at the modular junction of the CoCr femoral condyle and after long-stem total knee replacement (TKA), where mechanically-assisted fretting corrosion occurs in a similar fashion [15,16]. Various combinations of corrosion occur at these metallic junctions according to the alloy microstructure, and fretting/crevice and pitting corrosion occur more frequently [17]. Complex aggregates/agglomerates of metallic nanoparticles form upon mixing with organic species such as proteins/blood/cell debris *in vivo,* and are known to be potentially clinically relevant [18], but their formation has not been evaluated in pre-marketing studies and was not anticipated during the approval process by regulatory agencies nor in short-term post-marketing surveillance.

The release of metallic nano- and submicron particles of implant wear debris into the periprosthetic soft tissue and bone generated by various modalities of metal corrosion have been associated with adverse local tissue reactions/adverse reactions to metallic debris (ALTR/ARMD) [19–25]. The additional release of wear particles at the MAS/neck taper junction has been considered a key factor leading to the high revision rate of MoM large head (LH) THA due to ALTR/ARMD [26]. However, the roles played in the immunogenicity of the particles by the protein corona and possibly the complement system are still unclear [27–29].

Of particular interest is a model of non-MoM THA with CoCrMo DMN and Ti/Mo/Zr/Fe (TMZF) stem, which has been reported to generate agglomerates/aggregates of metallic nanoparticles only at the neck/stem junction, and has been associated with a poor survival rate at 5 years, with the occurrence of a high number of ALTR/ARMD irrespective of the patient's gender and age [30,31].

The cytotoxicity of single metal nanoparticles has been tested *in vitro* on a variety of cell types, including macrophages [32], lymphocytes [33,34], fibroblasts [35], and stem cells [36]. However, studies evaluating the cytotoxic effects of simultaneous exposure to complex metallic nanoparticles on macrophages, the expression of inflammatory cytokines, and their clinical implications are quite limited [37–39].

A recent clinical study revealed a correlation between quantitative and qualitative aspects of synovial inflammatory infiltrate and the complexity of the elemental composition of agglomerates/aggregates of metallic nanoparticles [40]. It was demonstrated that Co nanoparticles exhibited higher toxicity than Cr and Ti nanoparticles towards macrophages when they were administered *in vitro* [41–43]. However, their combined effects on macrophages resulting in cell death and expression of pro-inflammatory cytokines has not yet been evaluated in a mouse model *in vivo*.

This study was performed with two main objectives: a) to investigate whether the toxicity of clinically-relevant doses of a combination of commercially-available nanoparticles of Co, Cr, and Ti, administered to a human macrophage cell line *in vitro* and murine soft tissues *in vivo*, differed in comparison to their administration as nanoparticles of individual metals; b) to evaluate the morphological features and elemental analysis by transmission/scanning electron microscopy (TEM/SEM) *in vitro* and *in vivo* in a murine model, when exposed to single and combined metal nanoparticles.

2. Materials and methods

2.1. Metal nanoparticles

Metal nanoparticles (Co: purity 99.8%, mean size of 30 nm, Cr: purity 99%, mean size of 30 nm, Ti: purity 99.8%, mean size of 35 nm) were purchased from American Elements (Merelex Corp., Los Angeles, CA, USA); RPMI 1640 medium with glutamine, foetal bovine serum (FBS), and phosphate-buffered saline (PBS) were purchased from Thermo Fisher Scientific (Waltham, MA, USA). Hexamethyldisilazane was procured from Fluka (Gillingham, Dorset, UK). Trizol was obtained from Invitrogen (Carlsbad, CA, USA), TagDNA Polymerase High Fidelity was obtained from Life Technologies (Carlsbad, CA, USA), and silicon wafers were purchased from Agar Scientific Ltd (Stansted, Essex, UK). All other chemicals used were purchased from Sigma–Aldrich (St Louis, MO, USA).

2.2. In vitro cytotoxicity and nanoparticle analysis

2.2.1. Metal nanoparticle preparation

For cell culture, 10^{15} particles/mL were prepared and stored in 100% ethanol and kept at −20 °C to avoid aggregation/agglomeration and corrosion. The stock solution was diluted 1:1000 in RPMI 1640 medium supplemented with glutamine to obtain a concentration of 1×10^{12} particles (100 μg)/mL. The concentration of wear nanoparticles in the tissue in a clinical setting can vary significantly. It has been reported that under physiological conditions, the annual rate of nanoparticle production from MoM THA was approximately 1 mm^3 or 1×10^{13} in number [41]. A dose range of 1×10^9 to 1×10^{12} particles/mL was used in this study to assess the toxicity threshold. All prepared solutions of Co, Cr, and Ti nanoparticles and their combination were treated by sonication for 60 s to prevent possible agglomeration and suspension before use. The total number of particles used to make the stock solution and each tested concentration is listed in Table 1.

2.2.2. Neutral red cytotoxicity assay

Nanoparticle-induced cellular cytotoxicity was assessed in human THP-1 macrophages using the neutral red (Sigma–Aldrich) method [44]. In brief, THP-1 cells (American Type Culture Collection [ATCC], Manassas, VA, USA) were seeded into 96-well plates at a density of 1×10^4/well and the macrophages were activated using 50 nM phorbol 12-myristate 13-acetate phorbol 12-myristate 13-acetate (PMA, Sigma–Aldrich). After 72 h, the PMA-containing medium was discarded and the THP-1 cells were treated with individual Co, Cr, or Ti nanoparticles or their combination at different concentrations of 10^9, 10^{10}, 10^{11}, or 10^{12} nanoparticles/mL in RPMI 1640 complete medium. After 24 h of treatment with the nanoparticles, neutral red solution (0.33% neutral red in Dulbecco's PBS, Sigma–Aldrich) was added to the medium at a concentration of 10% and the cultures were incubated at 37 °C for 2 h. The cells were then observed under a light microscope and their images were captured with a digital camera. The plate was centrifuged for 5 min at 150×*g* and the medium was replaced with PBS. The plate was centrifuged again before the supernatant was removed, and the cells were solubilised

Table 1
Concentrations of nanoparticles (NPs) used for *in vitro* and *in vivo* studies.

Metal NP number/mL	Stock	Working solution			
	1×10^{13}/mL	1×10^{12}/mL	1×10^{11}/mL	1×10^{10}/mL	1×10^9/mL
Co	1 mg/mL	100 μg/mL	10 μg/mL	1 μg/mL	0.1 μg/mL
Cr	1 mg/mL	100 μg/mL	10 μg/mL	1 μg/mL	0.1 μg/mL
Ti	1 mg/mL	100 μg/mL	10 μg/mL	1 μg/mL	0.1 μg/mL
Co/Cr/Ti 1:1:1	1 mg/mL	100 μg/mL	10 μg/mL	1 μg/mL	0.1 μg/mL

in neutral red solubilisation solution (1% acetic acid in 50% ethanol; Sigma–Aldrich). After 10 min on a gyratory shaker, the absorbance was measured using a 'FLUO star Omega' microplate reader (BMG Labtech, Ortenberg, Germany) and the absorbance was spectrophotometrically measured at a wavelength of 540 nm (visible light). The background absorbance of the multi-well plates was measured at 690 nm and subtracted from the reading at 540 nm.

2.2.3. Phagocytosis of metal nanoparticles and their morphological/elemental analysis

Human THP-1 macrophages were used to evaluate phagocytosis of metal particles *in vitro*. In brief, THP-1 cells were seeded onto sterile 13 mm diameter Thermanox plastic coverslips (Thermo Fisher Scientific) at a density of 1×10^4 cells/well, placed in wells of a 24-well plate, and a suspension of 1×10^{11} nanoparticles/mL of Co, Cr or Ti, or 3.33×10^{10}/mL of each particle suspension mixed to give a combination of Co/Cr/Ti, was added to the cells. A control sample without nanoparticles was also included. The cells were incubated for 24 h at 37 °C, followed by fixation in 2.5% glutaraldehyde and fresh 10% paraformaldehyde (PFA) for 60 min. The samples were then dehydrated in increasing concentrations of ethanol. The plastic cover slips were dried to the critical point and carbon coated. The samples were then analysed using a Tescan S8000 SEM (Tescan-UK Ltd, Cambridge, UK) with an Ultim Extreme detector (Oxford Instruments, High Wycombe, UK) and the energy-dispersive X-ray spectroscopy (EDS) elemental analysis system (EDS software Aztec Version 4.2), to confirm the uptake and localisation of the nanoparticles and the proportion of each element.

For morphological and elemental analysis of the phagocytosed metal nanoparticles, cells were seeded into wells of a 6-well plate (1×10^4 cells/well) together with 10 μL of one metal/combination particle suspension and incubated for 48 h at 37 °C. A primary fix (2.5% glutaraldehyde solution (TAAB), fresh 10% PFA) was added to the wells for 60 min, then the rinsed cells were scraped and suspended in a secondary fix (2% aqueous osmium) for 60 min. The cells were stained in pellet form with 2% uranyl acetate and stored at 4 °C overnight. After dehydrating the cells in increasing concentrations of acetone, the cells were embedded as pellets in TAAB 812 hard embedding resin and polymerised for 12 h at 60 °C. The resin-embedded samples were sectioned using an RMC PowerTome and mounted onto copper grids, then 100 nm thick sections were obtained using a diamond knife. Images were taken for each sample using a JEOL JEM-1400 Flash electron microscope (Jeol Ltd., Tokyo, Japan).

2.3. In vivo RNA extraction and metal nanoparticle analysis

2.3.1. RNA extraction and metal nanoparticles analysis from the in vivo samples

The animal studies were approved by the Institutional Animal Research Committee of Tongji Medical College. All experimental steps involving animals were performed according to the rules and regulations of the Institutional Animal Care and Use Committee of Tongji Medical College. Briefly, 15 healthy male 8-week-old C57BL/6 J mice were randomly divided into five groups (n = 3 mice per group) as follows: Sham normal saline (NS) control (Sham); Co group (1×10^{12} particles/limb); Cr group (1×10^{12} particles/limb); Ti group (1×10^{12} particles/limb); and Co/Cr/Ti (1:1:1) group (1×10^{12} particles/limb). The animals were housed three per cage, maintained under a strict 12 h light, 12 h darkness cycle at 22 °C, and provided with standard mouse food pellets and free access to tap water. Under aseptic conditions, the mice were anesthetised by intraperitoneal injection of 1% pentobarbital and the skin of the hind limbs was shaved and sterilised with Iodophor. Solutions of nanoparticles of Co, Cr, Ti and their combination were sonicated for 60 min to prevent possible agglomeration, then the nanoparticle suspensions in NS were injected bilaterally into the gap between the tibialis anterior muscle and the tibial periosteum at a concentration of 1×10^{12} particles/limb. After 7 days, the mice from each group were euthanised by intracardial pentobarbital injection. Half of each right tibial soft tissue sample was snap frozen in liquid nitrogen for extraction of tissue RNA and the other half was fixed for examination by TEM/SEM. The left anterior tibial soft tissue specimens were fixed in 4% formaldehyde, processed through a standard cycle, embedded in paraffin, cut at 5 μm, and stained with haematoxylin and eosin (H&E) for examination by light microscopy.

2.3.2. RNA extraction and qPCR

Samples preserved in liquid nitrogen were used for RNA extraction. Briefly, the excised peri-tibial soft tissue was placed into a pre-cooled mortar, frozen in liquid nitrogen, and ground into a powder using a pestle. The tissue was then incubated in a centrifuge tube containing 1 mL Trizol (Invitrogen) for 10 min at 37 °C. Chloroform (0.2 mL) was then added. After manual shaking for 15 s, the sample was incubated at 37 °C for 10 min and centrifuged at 12,000×*g* for 15 min at 4 °C. After removal of the supernatant, 0.5 mL isopropanol was added and the tube was allowed to stand for 10 min at room temperature for RNA precipitation, followed by centrifugation at 12,000×*g* for 15 min at 4 °C. After removal of the supernatant, the RNA precipitate was washed once with 1 mL of 75% alcohol and centrifuged at 7500×*g* for 5 min at 4 °C. After removal of the supernatant, the RNA was dried at 37 °C for 10 min. The RNA was dissolved in 20 μL RNase-free water for quantitative real-time reverse transcription-PCR analysis. After vortex mixing, the RNA sample was warmed at 60 °C for 15 min to promote dissolution. cDNA was reverse transcribed from 1 μg of total RNA in a 20 μL reaction mixture containing 13 μL PCR buffer, 1 mM each of deoxynucleotide triphosphates, 1 unit/μL of RNase inhibitor, 1.25 μM random prier, 5 mM $MgCl_2$, and 5 units/μL of reverse transcriptase. The reaction mixture was incubated in a Veriti Thermal Cycler (Applied Biosystems, Waltham, MA, USA) at 25 °C for 10 min, 48 °C for 25 min, followed by 95 °C for 5 min.

The expression of tumour necrosis factor (TNF)-α, interleukin (IL)-1, IL-6, and hypoxia inducible factor (HIF)-1α was determined by regular PCR using TagDNA Polymerase High Fidelity (Cat#12346–086, Life Technologies). For each reaction, 2 μL of cDNA was added to a 25 μL reaction mixture containing PCR buffer and 0.04 units/μL of tag DNA polymerase, together with 0.4 μM of each primer. The reaction mixture was incubated in a Veriti Thermal Cycler (Applied Biosystems, Waltham, MA, USA) at 94 °C for 1 min, 60 °C for 1 min, followed by 72 °C for 1 min, for a total of 35 cycles.

2.3.3. Tissue preparation for electron microscopy (TEM/SEM)

For TEM/SEM analysis, the peri-tibial soft tissue was fixed in 2.5% glutaraldehyde in 0.1 M sodium cacodylate buffer at pH 7.4 for 10 min, trimmed to square tissue samples of 1 mm^3, and the fixation was continued at room temperature for 2 h, followed by rinsing twice with 0.1 M sodium phosphate buffer (pH 7.4) for 20 min. The specimens were fixed for a maximum of 3 days.

2.3.4. Statistical analyses

GraphPad software (Graphpad Software Inc., La Jolla, CA, USA) was used to perform statistical analyses. Two-way analysis of variance (ANOVA) was selected for the analysis of continuous variables. The Kruskal-Wallis test was used to analyse the data for inter-group comparisons. Differences with $p < 0.05$ were considered to be statistically significant (95% confidence intervals).

3. Results

3.1. Macrophage response to metal nanoparticles in vitro

The neutral red results of cytotoxicity assessments *in vitro* are shown in Fig. 1. Untreated human THP-1 macrophages are shown in Fig. 1A. Most of the cells are stained red (white arrows show representative cells) indicating endocytosis. THP-1 macrophages treated with Co metallic nanoparticles at the highest concentration (100 μg/mL) are shown in

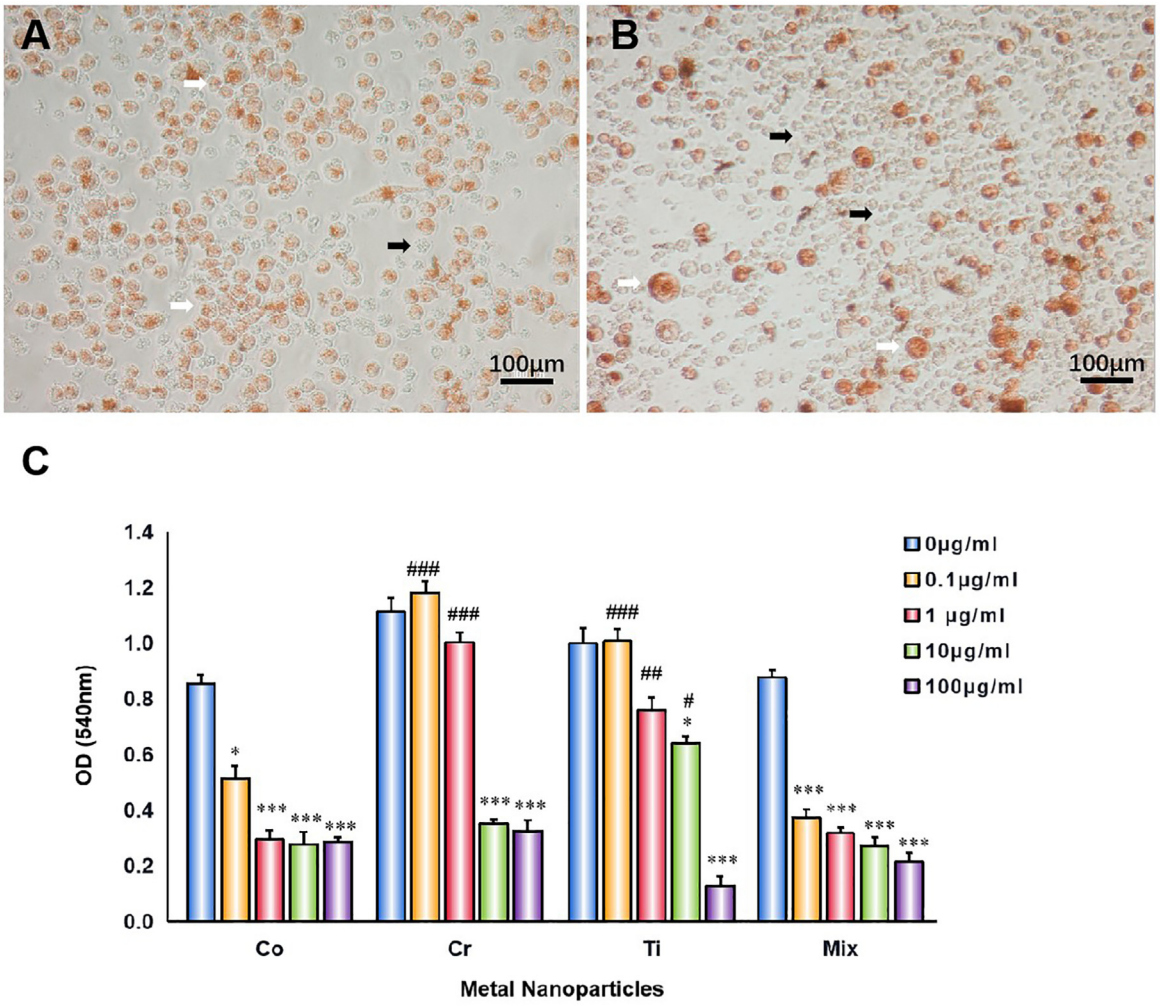

Fig. 1. Neutral Red staining and cytotoxicity assay. Neutral red staining of human THP-1 macrophages visualised by light microscopy: control group (A) and Co group at 100 μg/mL (B). White arrows indicate representative living cells and black arrows indicate representative dead cells. Bar = 100 μm. Cytotoxicity of different concentrations of Cr, Ti, Co, and Cr/Ti/Co on human THP-1 macrophages is shown in (C). The X-axis indicates different concentrations of added metal nanoparticles; Y-axis indicates the optical density (OD) of neutral red at an absorbance at 540 nm visible light. Asterisk (*) indicates comparison against the control group (*$p < 0.05$, **$p < 0.01$, ***$p < 0.01$); hash key (#) indicates comparison against the Mix group (#$p < 0.05$, ##$p < 0.01$, ###$p < 0.001$).

Fig. 1B. Most of the macrophages were non-viable and did not stain (black arrows show representative cells), indicating the loss of endocytic function. The small number of living macrophages stained dark red (white arrows) along with the presence of a few syncytial cells, indicate enhanced endocytosis.

The optical density (OD) of neutral red absorbance at 540 nm is shown in Fig. 1C. It represents an index of the cytotoxic effect of the three metallic nanoparticles (Co, Cr, Ti) and their combination Co/Cr/Ti (1:1:1) at concentrations of 0, 0.1, 1, 10, and 100 μg/mL, respectively.

Macrophage toxicity results were different for each metal nanoparticle (Fig. 1C). However the cytotoxicity was dose dependent for all the metal nanoparticle groups.

The Mix group showed the highest degree of macrophage toxicity. In comparison with the control group, there was a statistically significant reduction in the neutral red absorbance at all the tested doses ($p <$ 0.001). At the lower doses of 0.1 and 1 μg/mL, the Mix group also showed a significantly higher cytotoxicity than either the Cr or Ti group ($p <$ 0.001 and $p < 0.01$) and higher toxicity than the Co group at the lowest dose although the increase was not statistically significant. Among the Cr, Ti and Co groups, Co was more cytotoxic than Cr or Ti and showed significantly higher toxicity than the control group at all the tested doses ($p < 0.05$ and $p < 0.001$). The Cr and Ti groups showed significant cytotoxicity compared to the control group only at concentrations of 10 μg/mL and 100 μg/mL, with the Cr group at $p < 0.001$ for both doses and the Ti group at $p < 0.05$ and $p < 0.001$, respectively. The cytotoxicity assay was repeated in triplicate and showed consistent results. The effect was also validated using a murine macrophage cell line (RAW 264.7), and similar results were obtained (data not shown).

Elemental mapping analysis, and semi-quantification of the intracellular content of metallic nanoparticles are shown in Fig. 2. Not all macrophages were found to contain metal nanoparticles. The SEM images with colour-coded single metallic elements and the overlay images of macrophages that phagocytosed metal nanoparticles are shown in Fig. 2A. The metal nanoparticles (single metal or combination) were detected using EDS mapping. The semi-quantification of the intracellular content of each metallic element is shown in Fig. 2B.

The distribution of the metallic nanoparticles within a typical macrophage in the Co/Cr/TI group is shown in Fig. 2C and the corresponding highly electron-dense regions by backscattering spectroscopy are shown in Fig. 2D. Macrophages in this group were selected for point scanning of Co, Cr, and Ti content (Fig. 2E), and showed a Cr proportion that was 4-fold higher than that of Co or Ti ($p < 0.001$).

TEM analysis of the intracellular nanoparticles was performed on harvested human THP-1 macrophages cultured *in vitro* and on macrophages exposed to injected metal in the mouse peri-tibial soft tissue *in vivo*. The metal nanoparticles were phagocytosed by macrophages and

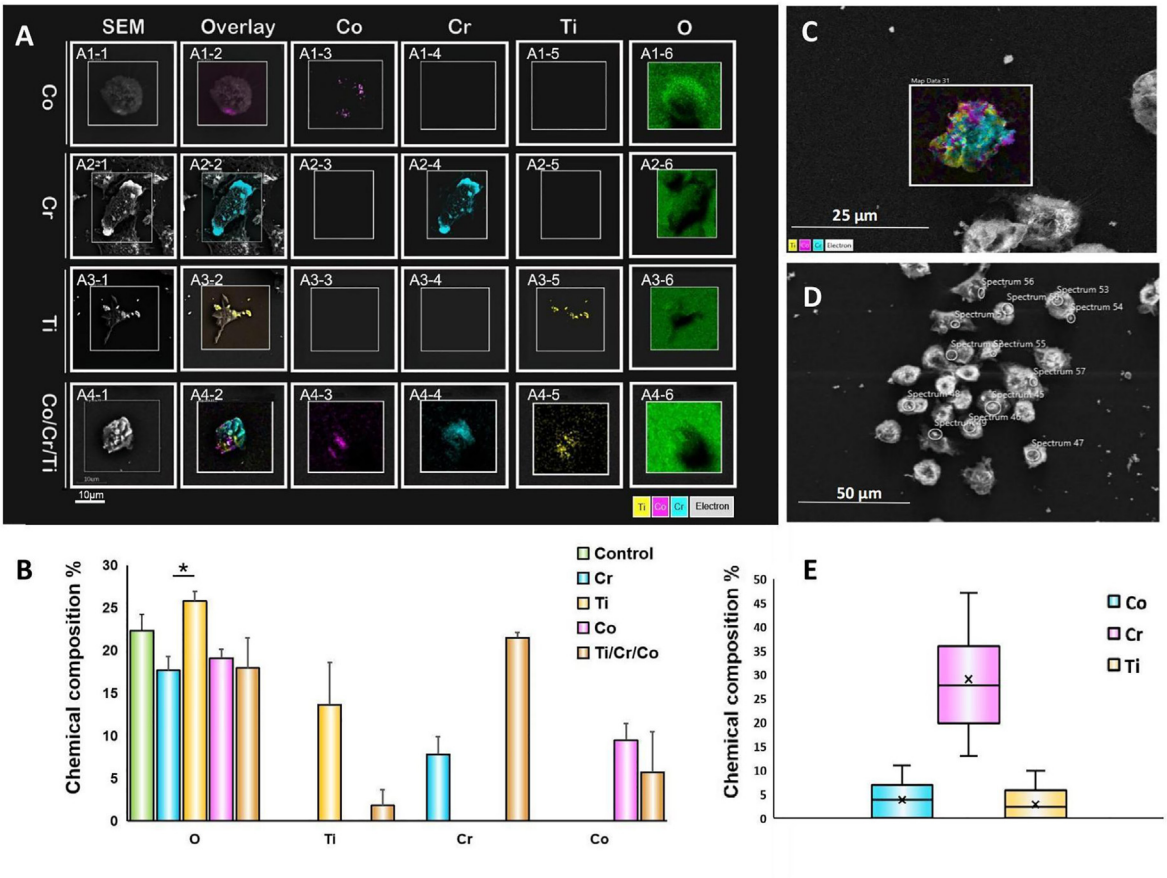

Fig. 2. Compositional analysis of macrophages following phagocytosis of metal nanoparticles. A. Scanning electron microscopy (SEM)/backscatter/energy-dispersive X-ray spectroscopy (EDS) element analysis of human THP-1 macrophages after phagocytosis of Co, Cr, Ti, or Co/Cr/Ti mixture. In the Co (A1, 1–5), Cr (A2, 1–5), and Ti (A3, 1–5) groups only one type of metal was detected, and in the Co/Cr/Ti combination group (A4, 1–5), all three elements were detected; oxygen (A1–A4, 6) was detected in all groups. B. Quantitative analysis of element composition shown in A. Within the regions of interest, oxygen levels in each group were similar, with the Ti group showing higher levels than the Cr group ($p < 0.05$). The content of Co (9.48 ± 1.92%), Cr (7.81 ± 2.11%) and Ti (13.62 ± 4.95%) in their corresponding groups were similar ($p > 0.05$). In the Co/Cr/Ti group, the contents of Co (5.70 ± 0.91%) and Ti (1.82 ± 0.62%) were lower than Co (9.48 ± 1.92%) and Ti (13.62 ± 4.95%), while Cr (21.48 ± 4.75%) was higher than in the Cr group (17.93 ± 1.87%). C. Intracellular distribution of Co, Cr and Ti nanoparticles in a typical macrophage of the Co/Cr/Ti group. D. Phagocytosed particles correspond to high electron density regions by backscattering spectroscopy. E. Point scanning shows as in D that the content of Cr in the endosomes of the Co/Cr/Ti group macrophages was around 4-fold higher than that of Co or Ti ($p < 0.001$).

stored in lysosomes in both the *in vitro* and *in vivo* samples (Fig. 3). In the groups cultured or injected with a single metal, the intracellular nanoparticles showed a distinct pattern of agglomeration/aggregation. In the Co group, the nanoparticles predominantly formed loose agglomerates/aggregates that were localised in the lysosomes (Fig. 3A and inset). In the Cr group, the nanoparticles formed dense agglomerates/aggregates, which were difficult to identify as individual particles (Fig. 3B and inset). In the Ti group, the nanoparticles formed dense agglomerates/aggregates with crystalloid features within the lysosomes (Fig. 3C and inset). In the Co/Cr/Ti group, when metal nanoparticles were mixed and added to the cell culture, a mixture of nanoparticles were arranged in complex aggregates and were detected in macrophages within 48 h. The morphology was very similar to those seen in the results from the *in vivo* experiment (Fig. 3D–F), wherein they formed a mixture of globular nanoparticles (Fig. 3D, E and G) with small and large agglomerates/aggregates of needle- or rod-shaped nanoparticles with occasional crystal-like shapes (Fig. 3D–H).

3.2. Macrophage response to the metal nanoparticles in vivo

Comparison of the expression of genes encoding the pro-inflammatory cytokines IL-1β, IL-6, TNF-α and IL-8 in the Co, Cr, Ti, and Co/Cr/Ti mouse groups with the control group at 7 days after injection is presented in Fig. 4.

The Ti group did not show a statistically-significant increase in expression of the tested genes. There was a modest increase in the expression of IL-1β, TNF-α and IL-8 in the Cr group ($p < 0.05$), while in the Co and the Co/Cr/Ti groups, there was a marked increase in the expression of all the four tested genes ($p < 0.01$).

EDS element mapping and point-scan elemental analysis of typical macrophages in the Co/Cr/Ti group are presented in Fig. 5. A distinct pattern of the distribution of metallic nanoparticles was detected for each metal. Loose agglomerates of circular nanoparticles were predominantly composed of Co (A1–2, A2–2, B2–2); needle-shaped dense agglomerates/aggregates were predominantly composed of Cr (A1–3), and crystal-like dense agglomerates/aggregates were predominantly composed of Ti (B1–4, B2–4). These findings were verified by point scan analysis in the presence of only a small percentage of other metals (Fig. 5C).

4. Discussion

The occurrence of clinical complications of arthroplasty arising from metal debris has been reported to be associated with a complex inflammatory reaction, characterised by delayed hypersensitivity, potentially of different subtypes depending on the chemical–physical properties of the wear particles and the host's immunological profile [45]. The cause could be attributed to nanoparticulate wear materials generated by various modalities of metal corrosion and interaction with the host synovial fluid

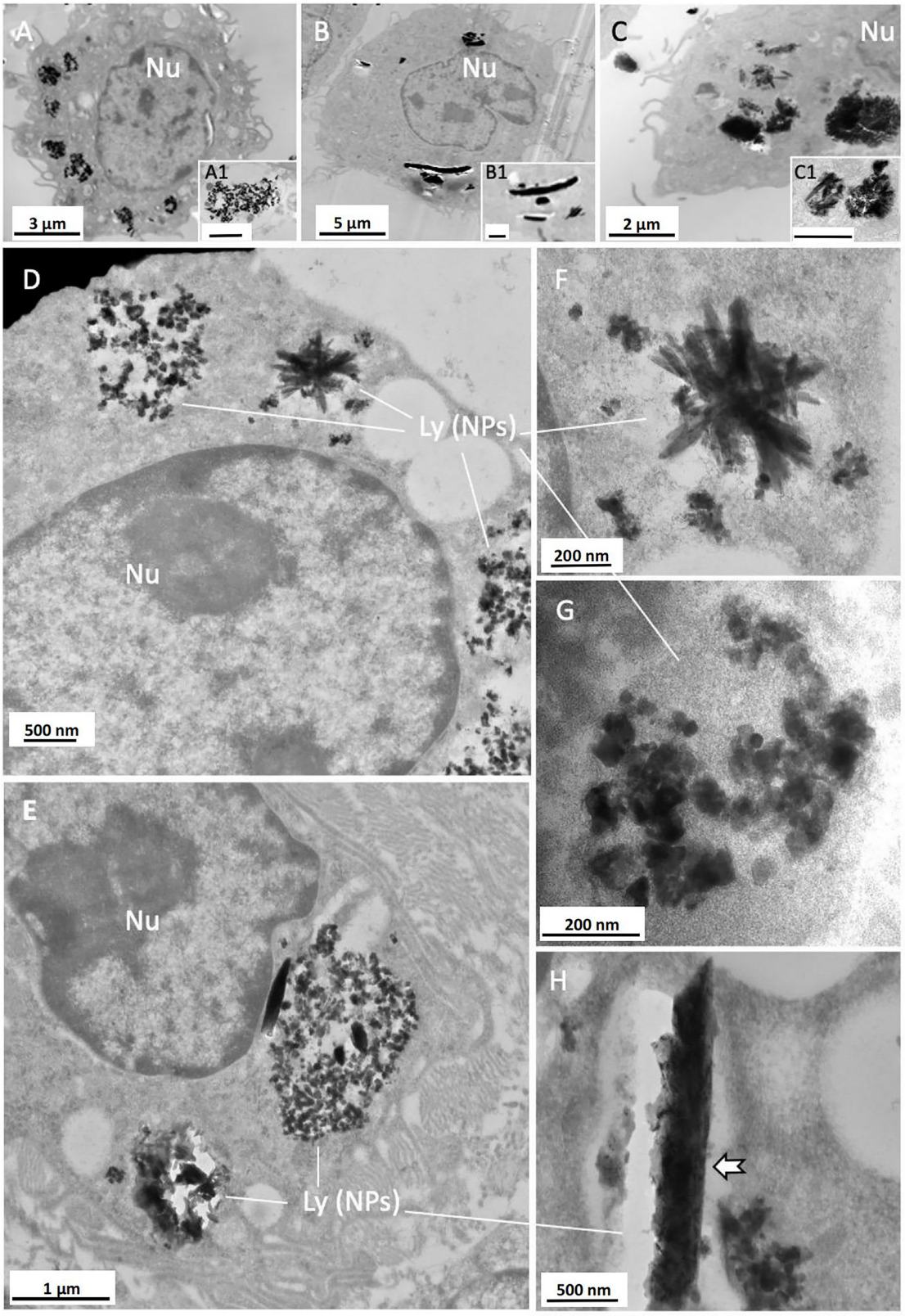

Fig. 3. TEM analysis of intracellular metallic nanoparticles *in vitro*. Morphology of intracellular Co, Cr and Ti nanoparticles phagocytosed by human THP-1 macrophages over 48 h *in vitro* (A–C with insets) and Balb/C mouse macrophages after 7 days exposure *in vivo* (D–H). A. Co globular nanoparticles (magnification in inset); B. Cr agglomerates/aggregates of nanoparticles in large clusters (magnification in inset); C, agglomerates/aggregates of Ti nanoparticles with crystal-like shape (magnification in inset); D and E, the combination of Co/Cr/Ti shows complex agglomerates/aggregates of nanoparticles in lysosomes. F, crystal-like and globular nanoparticles; G, agglomerates/aggregates of globular nanoparticles of variable electron density; H, large agglomerates/aggregates of nanoparticles forming a rod-like structure (arrow). Nu, cell nuclei. Ly (NPs), lysosomes containing metallic nanoparticles. Scale bars: A1, B1, C1 = 1 µm.

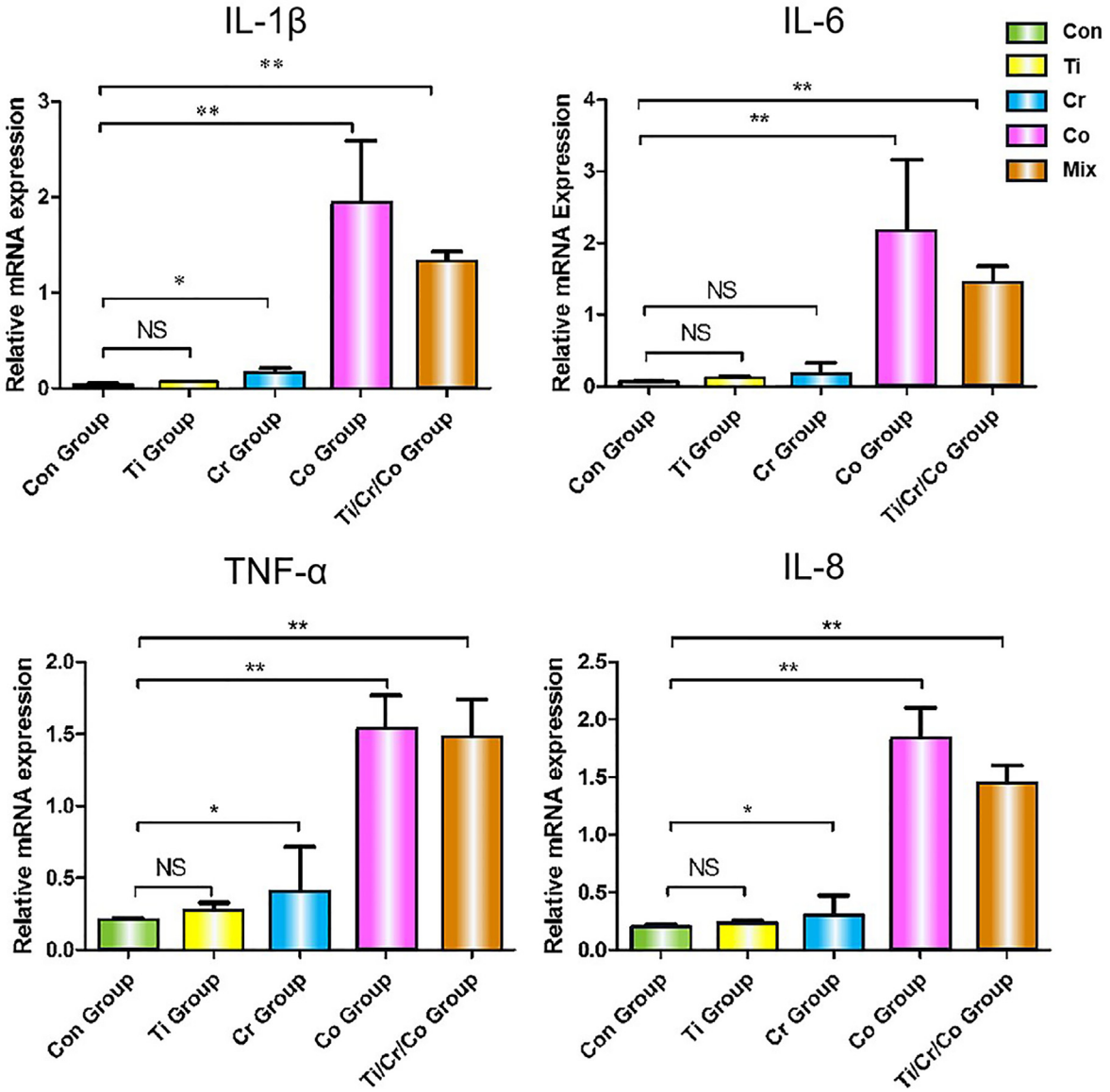

Fig. 4. QPCR analysis of pro-inflammatory cytokines. IL-1β, IL-6, TNF-α and IL-8 mRNA expression after 7 days implantation of Co, Cr, Ti, and Co/Cr/Ti groups in comparison with the control group. NS, not significant; $*p < 0.05$, $**p < 0.01$.

and organic matter, stimulating an adaptive immunological response. The expression of pro-inflammatory cytokines by macrophages after phagocytosis/endocytosis of metallic nanoparticles *in vitro* has been well documented, especially when Co is present in the particulate material [46]. The characterisation of the intracellular agglomerates/aggregates of nanoparticles by electron microscopy coupled with elemental analysis is instrumental for understanding cell death modalities and qualitative and quantitative expression of pro-inflammatory cytokines. This may contribute to the recruitment of lymphocytic infiltrates causing soft tissue necrosis after a short period of implantation, and recruitment of bone marrow macrophages leading to clinically-significant osteolysis after a longer period of implantation [45].

In this study, we selected a proximal peri-tibial soft tissue site for injection instead of a hip or knee joint for the following reasons: (a) single injection of metallic particles was insufficient to induce synovial papillary/polypoid stromal proliferation of the synovium and lymphocytic reaction because of the use of metallic particles that were not generated by corrosion in the clinical setting; (b) absence of a hip implant providing continuous generation of wear particles with progressive reaction of the synovial membrane; (c) rapid macrophage response to foreign particles and easier retrieval and processing of the tissues for TEM/SEM particle analysis. Our rationale was validated by a recent study in which no stromal proliferation or lymphocytic response were detected after a single intra-articular injection of commercially-available metallic particles in a mouse model [47].

This study demonstrated that the administration of nanoparticles of three different metals mimicking wear particles from the hip head (CoCr) and neck (Ti) junction and dual neck (CoCr) and stem (Ti) was more toxic than nanoparticles of any of the individual metals, required lower concentrations to induce similar levels of toxicity, and confirmed the validity of TEM/SEM techniques for intracellular particle analysis *in vitro* and *in vivo*.

The treatment of macrophages with particulate wear materials in post-marketing studies of orthopaedic implants should match the composition of the wear particles generated in the patient's joints, and must be identified by TEM/SEM particle nano-analysis of the macrophages present in specimens of periprosthetic tissue retrieved from subjects with implant revision.

In this study, despite using commercially-available metallic nanoparticles of uniform size, the combination of Co/Cr/Ti nanoparticles was

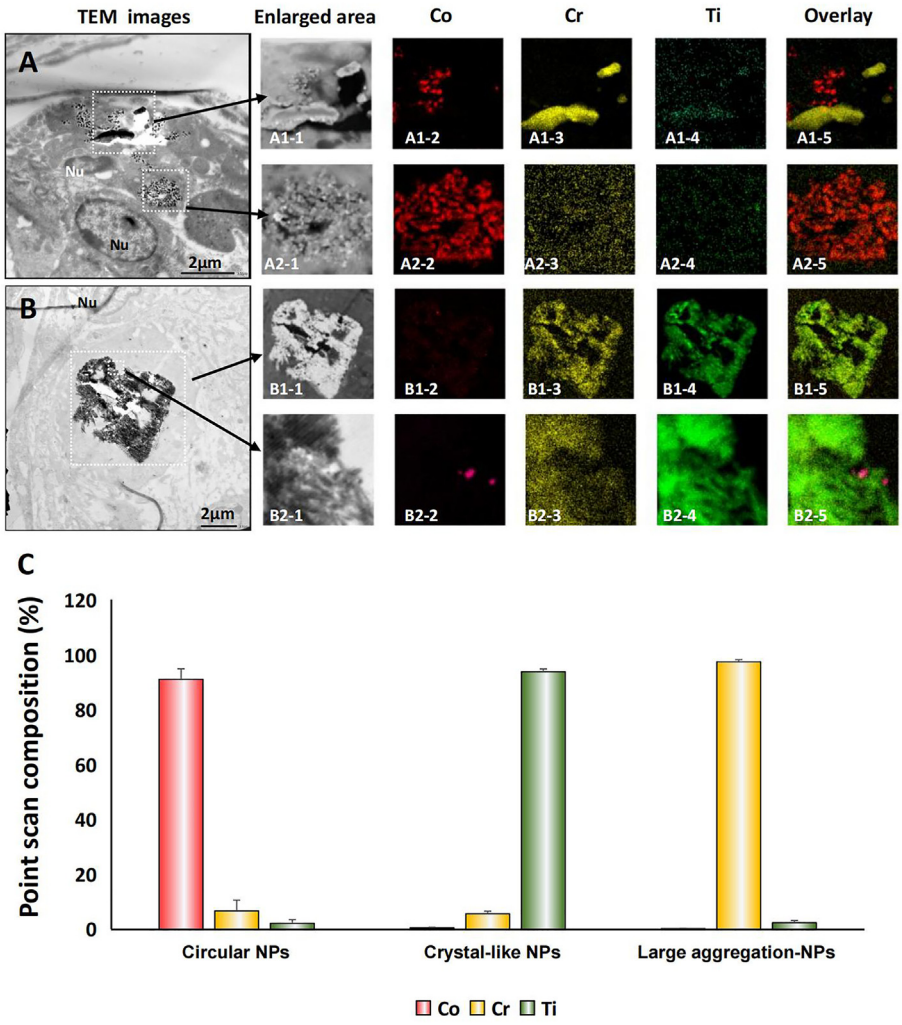

Fig. 5. EDS element mapping and point-scan element analysis of metallic nanoparticles *in vivo*. A, B. Intracellular metallic nanoparticles of the Co/Cr/Ti group, distributed as loose or needle-shaped/crystal-like agglomerates/aggregates. Circular nanoparticles were predominantly composed of Co (A1–2, A2–2, B2–2); needle-shaped agglomerates/aggregates were predominantly composed of Cr (A1–3); crystal-like agglomerates/aggregates were predominantly composed of Ti (B1–4, B2–4). C. Point scans of the three types of particles. Morphological features of the metallic nanoparticle aggregates corresponded to a predominant metal element; only a small percentage of other metals was present.

found to be more cytotoxic than the nanoparticles generated from the individual metals *in vitro*. These findings were similar to those from a clinical study that reported increased macrophage necrosis according to the complexity of the metallic wear nanoparticles in retrieved synovial tissue from subjects undergoing implant revision [40]. The results also confirmed that Co nanoparticles were more cytotoxic at any of the tested concentrations than those composed of Cr or Ti [27,35]. This finding indicated that at comparable particle size (30–35 nm), the elemental composition of the nanoparticles was the most important factor influencing cytotoxicity. The mechanism of cytotoxicity of the metal particles is considered to be dependent on multiple molecular and physicochemical mechanisms [48] and ion release [41]. However, a recent study on a murine model suggested a more significant role of the particles over the ions [47].

Cell death occurs after intracellular uptake of particles through: (a) acidification, with lysosomal pH less than 4; (b) oxidation, since reactive oxygen species can be released as H_2O_2, $^{\bullet}O_3^-$, HO^-, or $^{\bullet}OH$ to oxidise the engulfed particles; and (c) digestion by proteinases, in case of formation of metal–organic particulate material. Therefore, the phagosomes may simultaneously contain metal nanoparticles, metal oxidants, and salts. The formation of salts is due to the presence of carbonate (CO_3^{2-}), phosphate (PO_3^{3-}) and chloride (Cl^-) in physiological body fluids. Co compounds are more soluble than those of Cr and Ti. This could explain in part why more ions were released from the Co particles into the cytoplasm and the extracellular environment. It was proposed that Co nanoparticles activated the HIF pathway by depleting intracellular ascorbate, leading to the stabilisation of HIF and pathway activation, suggesting a strong ROS-independent role of HIF activation in Co-nanoparticle-induced cytotoxicity [49]. However, a recent study reported that by knocking out HIF-1α, the cytotoxic effects of Co were more pronounced on macrophages [50]. The type(s) of cell necrosis involved in nanoparticle-mediated toxicity were investigated only very recently *in vitro* [51] and have not yet been studied in clinical specimens to determine its possible contribution to the inflammatory reaction, especially soft tissue necrosis [52].

An unexpected finding was the predominance of Cr particles in the phagosomes of the mixed group. Although equal amounts of Co, Cr and Ti nanoparticles were added to the culture medium, the proportion of intracellular Cr was 4-fold higher than that of Co and Ti (Fig. 3B, E). A high content of Cr has also been observed in clinical samples, although the explanation was that under physiological conditions, the majority of wear particles generated at the bearing surface were composed of Cr, and Co was present only in cases of edge loading/excessive wear [11,53]. It has been speculated that there might be different modalities and rates of particle phagocytosis for each metal [54,55], however, this needs to be confirmed by confocal laser scanning microscopy [56].

TEM/SEM particle analysis showed a distinct, metal-specific pattern of agglomeration/aggregation of the intracellular nanoparticles, with implications that were potentially relevant to their cytotoxicity and immunogenicity, observed *in vitro* and *in vivo*. So far, these have not been explored by studies investigating experimental metal toxicity.

Furthermore, this study showed that the dose of 1×10^{12} particles of Co and the combination of Co/Cr/Ti significantly increased the expression of all the pro-inflammatory cytokines (IL-1α, IL-6, IL-8 and TNF-α)

that were evaluated *in vivo*. In the mixed group, only one third of the particles consisted of Co, which raised the interesting question of the threshold value or the differing effects of Co particles when in combination with other metals. Ti is known to be a relatively inert material [57]. However, it is unclear whether Ti nanoparticles increased the cytotoxicity/release of pro-inflammatory cytokines when associated with other metals, and the underlying mechanism needs further investigation.

Examination of the change in macrophage motility induced by metallic wear nanoparticles is key to understanding their migration from the synovium to the bone marrow, which causes osteolysis, the predominant and long-term adverse reaction in arthroplasty. It has been reported that exposure to Co rather than Cr nanoparticles reduced macrophage motility and caused macrophage retention by restructuring the cytoskeleton and inhibiting cell migration [58]. However, the results of this elegant study were not fully supported by histological examination of bone specimens from MoM hip resurfacing arthroplasty implants subjected to clinically-significant osteolysis with the loosening of implant components. Such specimens are expected to show massive invasion of the bone marrow by macrophages containing a mixture of Cr and Co rich particles, which is confirmed by high serum values of Co and Cr [45]. The discrepancy between the *in vitro* data and clinical behaviour of macrophages implies differences in the host response which need to be investigated in depth. Future studies need to compare the *in vitro* results with the macrophage response in patients with revised MoM hip resurfacing arthroplasty implants and demonstrate similar release of wear particles and presence/absence of macrophage-driven osteolysis.

The combined nanoparticle group with one third of the dose of each of Co, Cr and Ti showed the highest cytotoxicity and expression of inflammatory factors when compared with other single-element nanoparticles. Furthermore, significant cytotoxic effects of the combined metal nanoparticles were also observed at low concentrations (1×10^9 and 1×10^{10} particles/mL), which corroborated clinical data that reported that nanoparticles composed of several metals including Co were more cytotoxic than single-metal nanoparticles, either composed of Cr or Ti.

Finally, the morphology of macrophage phagocytosis and metal nanoparticles within the phagosomes from the *in vivo* mouse model were similar to the ultrastructural features observed in clinical samples [40]. However, these results are still preliminary and require a larger number of observations.

Recently, the role of macrophage phenotypes in response to biomaterials has been studied [59]. Rao et al. found higher expression of pro-inflammatory M1 macrophages in revision tissues [60]. Our previous study showed that Co nanoparticles caused pro-inflammatory expression of macrophages [61]. Since macrophage phenotype and polarisation is a dynamic process, it will be interesting to understand the role of metal nanoparticles in shifting local tissue inflammation and regeneration [62].

In further studies, we plan to address some of the issues pertaining to the *in vitro* findings and employ a simplistic experimental model mimicking the conditions from the clinical setting. We are particularly interested in the use of macrophages derived from patients undergoing joint replacement and implant-derived loose wear particle agglomerates/aggregates for observing phagocytic or endocytic processes, and macrophage subtype [63] and motility on different substrates. Furthermore, the *in vivo* model needs to be optimised to enable the injection of clinically-relevant nanoparticles into the joint or bone marrow.

There are several limitations associated with the current study. The metal nanoparticles used in this study were from commercial sources and were not generated by metal corrosion, as is found in the clinical setting. The macrophage response to the injection of metal nanoparticles in the peri-tibial soft tissue may differ from that occurring in the synovial membrane and macrophage typing and modalities of cell death were also not evaluated in depth. In addition we only tested a limited number of inflammatory cytokines in this study.

5. Conclusions

In conclusion, this study demonstrates that the combination of Co/Cr/Ti nanoparticles is more toxic to macrophages than single-metal nanoparticles *in vitro* and results in enhanced levels of pro-inflammatory cytokines *in vivo*. After phagocytosis, Cr compounds are more likely to accumulate intracellularly. The murine model used in this study shows its potential usefulness for rapid testing with a single injection of metal nanoparticles in peri-tibial soft tissue for TEM/SEM analysis of intracellular particle content and release of pro-inflammatory cytokines *in vivo* in pre-/post-marketing studies for unintended wear particle debris.

Credit author statement

Zhao Liu: experimental design, performance, data analysis of THP-1 *in vitro* tests. Manuscript writing and revision, graphs, and figure preparation. Hui Liu: *in vivo* experimental design and performance, sample processing, qPCR analysis and manuscript preparation. Rachel Vowden: *in vitro* experimental design and performance using RAW 246.7 cells. SEM and TEM analysis. Louise Hughes: experimental design, supervision, SEM/EDS analysis, manuscript preparation. Dahu Qi: support of *in vivo* experiments. Wendy Francis: support of *in vitro* experiments and supervision. Giorgio Perino: initial concept, supervision, manuscript preparation and revision, consumable and clinical support. Ryan Pink: student supervision and experimental support. Jun Xiao: student supervision and consumable support. Bin Li: project oversight, manuscript revision, supervision, and consumable support. Zhidao Xia: project design and oversight, *in vitro* and *in vivo* experiments, data analysis, manuscript writing and revision, preparation of figures and graphs, supervision, and consumable support.

Declaration of competing interest

We declare that they have no known competing financial interests or personal relationships that could have appeared to influence the work reported in this paper.

Acknowledgements

We would like to acknowledge the Thackray Medical Research Trust for financial support of a MSc studentship of this project and Christopher von Ruhland, PhD for samples preparation for TEM/SEM analysis.

References

[1] Learmonth ID, Young C, Rorabeck C. The operation of the century: total hip replacement. Lancet 2007;370(9597):1508–19.
[2] Amstutz HC, Le Duff MJ. Hip resurfacing: history, current status, and future. Hip Int 2015;25(4):330–8.
[3] Xia R, Zhai Z, Zhang J, Yu D, Wang L, Mao Y, et al. Verification and clinical translation of a newly designed "Skywalker" robot for total knee arthroplasty: a prospective clinical study. J Orthop Translat 2021;29:143–51.
[4] Johal S, Nakano N, Baxter M, Hujazi I, Pandit H, Khanduja V. Unicompartmental knee arthroplasty: the past, current controversies, and future perspectives. J Knee Surg 2018;31(10):992–8.
[5] Flatow EL, Harrison AK. A history of reverse total shoulder arthroplasty. Clin Orthop Relat Res 2011;469(9):2432–9.
[6] Cao H, Guan H, Lai Y, Qin L, Wang X. Review of various treatment options and potential therapies for osteonecrosis of the femoral head. J Orthop Translat 2016;4:57–70.
[7] Gougoulias NE, Khanna A, Maffulli N. History and evolution in total ankle arthroplasty. Br Med Bull 2009;89:111–51.
[8] McBeath R, Osterman AL. Total wrist arthroplasty. Hand Clin 2012;28(4):595–609.
[9] Yuan L, Ding S, Wen C. Additive manufacturing technology for porous metal implant applications and triple minimal surface structures: a review. Bioact Mater 2019;4(1):56–70.
[10] Chen C-H, O'Keefe R. Clinical translation and application in orthopaedics. J Orthop Translat 2018;12:A3–4.
[11] Kovochich M, Fung ES, Donovan E, Unice KM, Paustenbach DJ, Finley BL. Characterization of wear debris from metal-on-metal hip implants during normal

wear versus edge-loading conditions. J Biomed Mater Res B Appl Biomater 2018; 106(3):86–996.
[12] Lavigne M, Belzile EL, Roy A, Morin F, Amzica T, Vendittoli PA. Comparison of whole-blood metal ion levels in four types of metal-on-metal large-diameter femoral head total hip arthroplasty: the potential influence of the adapter sleeve. J Bone Joint Surg Am 2011;93(Suppl 2):128–36.
[13] Langton DJ, Sidaginamale RP, Avery P, Waller S, Tank G, Lord J, et al. Retrospective cohort study of the performance of the Pinnacle metal on metal (MoM) total hip replacement: a single-centre investigation in combination with the findings of a national retrieval centre. BMJ Open 2016;6(4):e007847–59.
[14] Buente D, Huber G, Bishop N, Morlock M. Quantification of material loss from the neck piece taper junctions of a bimodular primary hip prosthesis. A retrieval study from 27 failed Rejuvenate bimodular hip arthroplasties. Bone Joint Lett J 2015;97-B(10):1350–7.
[15] Perino G, De Martino I, Zhang L, Xia Z, Gallo J, Natu S, et al. The contribution of the histopathological examination to the diagnosis of adverse local tissue reactions in arthroplasty. EFORT Open Reviews 2021;6(6):399–419.
[16] Christiner T, Pabbruwe MB, Kop AM, Parry J, Clark G, Collopy D. Taper corrosion and adverse local tissue reactions in patients with a modular knee prosthesis. JB JS Open Access 2018;3(4):e0019–26.
[17] Pourzal R, Hall DJ, Ehrich J, McCarthy SM, Mathew MT, Jacobs JJ, et al. Alloy microstructure dictates corrosion modes in THA modular junctions. Clin Orthop Relat Res 2017;475(12):3026–43.
[18] Jacobs JJ, Gilbert JL, Urban RM. Corrosion of metal orthopaedic implants. J Bone Joint Surg Am 1998;80(2):268–82.
[19] Davies AP, Willert HG, Campbell PA, Learmonth ID, Case CP. An unusual lymphocytic perivascular infiltration in tissues around contemporary metal-on-metal joint replacements. J Bone Joint Surg Am 2005;87(1):18–27.
[20] Huber M, Reinisch G, Trettenhahn G, Zweymuller K, Lintner F. Presence of corrosion products and hypersensitivity-associated reactions in periprosthetic tissue after aseptic loosening of total hip replacements with metal bearing surfaces. Acta Biomater 2009;5(1):172–80.
[21] Langton DJ, Jameson SS, Joyce TJ, Hallab NJ, Natu S, Nargol AV. Early failure of metal-on-metal bearings in hip resurfacing and large-diameter total hip replacement: a consequence of excess wear. J Bone Joint Surg Br 2010;92(1):38–46.
[22] Natu S, Sidaginamale RP, Gandhi J, Langton DJ, Nargol AV. Adverse reactions to metal debris: histopathological features of periprosthetic soft tissue reactions seen in association with failed metal on metal hip arthroplasties. J Clin Pathol 2012; 65(5):409–18.
[23] Georgiev GP, Tanchev PP, Zheleva Z, Kinov P. Comparison of topical and intravenous administration of tranexamic acid for blood loss control during total joint replacement: review of literature. J Orthop Translat 2018;13:7–12.
[24] Hu CY, Yoon T-R. Recent updates for biomaterials used in total hip arthroplasty. J Orthop Translat 2018;22(1):1–12.
[25] Ricciardi BF, Nocon AA, Jerabek SA, Wilner G, Kaplowitz E, Goldring SR, et al. Histopathological characterization of corrosion product associated adverse local tissue reaction in hip implants: a study of 285 cases. BMC Clin Pathol 2016;16:3–19.
[26] Monopoli MP, Aberg C, Salvati A, Dawson KA. Biomolecular coronas provide the biological identity of nanosized materials. Nat Nanotechnol 2012;7(12):779–86.
[27] Fleischer CC, Payne CK. Nanoparticle-cell interactions: molecular structure of the protein corona and cellular outcomes. Acc Chem Res 2014;47(8):2651–9.
[28] Chen F, Wang G, Griffin JI, Brenneman B, Banda NK, Holers VM, et al. Complement proteins bind to nanoparticle protein corona and undergo dynamic exchange in vivo. Nat Nanotechnol 2017;12(4):387–93.
[29] Zhang L, Haddouti E-M, Welle K, Burger C, Kabir K, Schildberg FA. Local cellular responses to metallic and ceramic nanoparticles from orthopedic joint arthroplasty implants. Int J Nanomed 2020;15:6705–20.
[30] Meftah M, Haleem AM, Burn MB, Smith KM, Incavo SJ. Early corrosion-related failure of the rejuvenate modular total hip replacement. J Bone Joint Surg Am 2014;96(6):481–7.
[31] Nawabi DH, Do HT, Ruel A, Lurie B, Elpers ME, Wright T, et al. Comprehensive analysis of a recalled modular total hip system and recommendations for management. J Bone Joint Surg Am 2016;98(1):40–7.
[32] Lanone S, Rogerieux F, Geys J, Dupont A, Maillot-Marechal E, Boczkowski J, et al. Comparative toxicity of 24 manufactured nanoparticles in human alveolar epithelial and macrophage cell lines. Part Fibre Toxicol 2009;6:14–25.
[33] Tirumala V, Klemt C, Xiong L, Chen W, van den Kieboom J, Kwon Y-M. Diagnostic utility of platelet count/lymphocyte count ratio and platelet count/mean platelet volume ratio in periprosthetic joint infection following total knee arthroplasty. J Orthop Translat 2021;36(1):291–7.
[34] Posada OM, Tate RJ, Grant MH. Toxicity of cobalt-chromium nanoparticles released from a resurfacing hip implant and cobalt ions on primary human lymphocytes in vitro. J Appl Toxicol 2015;35(6):614–22.
[35] Behl B, Papageorgiou I, Brown C, Hall R, Tipper JL, Fisher J, et al. Biological effects of cobalt-chromium nanoparticles and ions on dural fibroblasts and dural epithelial cells. Biomaterials 2013;34(14):3547–58.
[36] Preedy EC, Perni S, Prokopovich P. Cobalt and titanium nanoparticles influence on mesenchymal stem cell elasticity and turgidity. Colloids Surf B Biointerfaces 2017; 157:146–56.
[37] Scharf B, Clement CC, Zolla V, Perino G, Yan B, Elci SG, et al. Molecular analysis of chromium and cobalt-related toxicity. Sci Rep 2014;4:5729–40.
[38] Kolatat K, Perino G, Wilner G, Kaplowitz E, Ricciardi BF, Boettner F, et al. Adverse local tissue reaction (ALTR) associated with corrosion products in metal-on-metal and dual modular neck total hip replacements is associated with upregulation of interferon gamma-mediated chemokine signaling. J Orthop Res 2015;33(10): 1487–97.
[39] Catelas I, Lehoux EA, Ning Z, Figeys D, Baskey SJ, Beaule PE. Differential proteomic analysis of synovial fluid from hip arthroplasty patients with a pseudotumor vs. Periprosthetic osteolysis. J Orthop Res 2018;36(7):1849–59.
[40] Xia Z, Ricciardi BF, Liu Z, von Ruhland C, Ward M, Lord A, et al. Nano-analyses of wear particles from metal-on-metal and non-metal-on-metal dual modular neck hip arthroplasty. Nanomedicine 2017;13(3):1205–17.
[41] Kwon YM, Xia Z, Glyn-Jones S, Beard D, Gill HS, Murray DW. Dose-dependent cytotoxicity of clinically relevant cobalt nanoparticles and ions on macrophages in vitro. Biomed Mater 2009;4(2):25018–25.
[42] VanOs R, Lildhar LL, Lehoux EA, Beaule PE, Catelas I. In vitro macrophage response to nanometer-size chromium oxide particles. J Biomed Mater Res B Appl Biomater 2014;102(1):149–59.
[43] Valles G, Gonzalez-Melendi P, Gonzalez-Carrasco JL, Saldana L, Sanchez-Sabate E, Munuera L, et al. Differential inflammatory macrophage response to rutile and titanium particles. Biomaterials 2006;27(30):5199–211.
[44] Hu W, Culloty S, Darmody G, Lynch S, Davenport J, Ramirez-Garcia S, et al. Neutral red retention time assay in determination of toxicity of nanoparticles. Mar Environ Res 2015;111:158–61.
[45] Perino G, De Martino I, Zhang L, Xia Z, Gallo J, Natu S, et al. The contribution of the histopathological examination to the diagnosis of adverse local tissue reactions in arthroplasty. EFORT Open Rev 2021;6(6):399–419.
[46] Horev-Azaria L, Kirkpatrick CJ, Korenstein R, Marche PN, Maimon O, Ponti J, et al. Predictive toxicology of cobalt nanoparticles and ions: comparative in vitro study of different cellular models using methods of knowledge discovery from data. Toxicol Sci 2011;122(2):489–501.
[47] Cheng X, Dirmeier SC, Hasselt S, Baur-Melnyk A, Kretzer JP, Bader R, et al. Biological reactions to metal particles and ions in the synovial layer of mice. Materials 2020;13(5):1044–57.
[48] Huang YW, Cambre M, Lee HJ. The toxicity of nanoparticles depends on multiple molecular and physicochemical mechanisms. Int J Mol Sci 2017;18(12):2702–14.
[49] Nyga A, Hart A, Tetley TD. Importance of the HIF pathway in cobalt nanoparticle-induced cytotoxicity and inflammation in human macrophages. Nanotoxicology 2015;9(7):905–17.
[50] Zhang L, Haddouti E-M, Beckert H, Biehl R, Pariyar S, Rüwald JM, et al. Investigation of cytotoxicity, oxidative stress, and inflammatory responses of tantalum nanoparticles in THP-1-derived macrophages. Mediat Inflamm 2020; 2020:3824593–606.
[51] Zerboni A, Bengalli R, Fiandra L, Catelani T, Mantecca P. Cellular mechanisms involved in the combined toxic effects of diesel exhaust and metal oxide nanoparticles. Nanomaterials 2021;11(6):1437–52.
[52] Vanlangenakker N, Vanden Berghe T, Vandenabeele P. Many stimuli pull the necrotic trigger, an overview. Cell Death Differ 2012;19(1):75–86.
[53] Bijukumar DR, Segu A, Souza JCM, Li X, Barba M, Mercuri LG, et al. Systemic and local toxicity of metal debris released from hip prostheses: a review of experimental approaches. Nanomedicine 2018;14(3):951–63.
[54] Zhu M, Nie G, Meng H, Xia T, Nel A, Zhao Y. Physicochemical properties determine nanomaterial cellular uptake, transport, and fate. Acc Chem Res 2013;46(3): 622–31.
[55] Behzadi S, Serpooshan V, Tao W, Hamaly MA, Alkawareek MY, Dreaden EC, et al. Cellular uptake of nanoparticles: journey inside the cell. Chem Soc Rev 2017; 46(14):4218–44.
[56] Richards DM, Endres RG. The mechanism of phagocytosis: two stages of engulfment. Biophys J 2014;107(7):1542–53.
[57] Chellappa M, Anjaneyulu U, Manivasagam G, Vijayalakshmi U. Preparation and evaluation of the cytotoxic nature of TiO2 nanoparticles by direct contact method. Int J Nanomed 2015;10(Suppl 1):31–41.
[58] Xu J, Yang J, Nyga A, Ehteramyan M, Moraga A, Wu Y, et al. Cobalt (II) ions and nanoparticles induce macrophage retention by ROS-mediated down-regulation of RhoA expression. Acta Biomater 2018;72:434–46.
[59] Kzhyshkowska J, Gudima A, Riabov V, Dollinger C, Lavalle P, Vrana N, et al. Macrophage responses to implants: prospects for personalized medicine. J Leukoc Biol 2015;98(6):953–62.
[60] Rao AJ, Gibon E, Ma T, Yao Z, Smith L, Goodman S, et al. Revision joint replacement, wear particles, and macrophage polarization. Acta Biomater 2012; 8(7):2815–23.
[61] Francis WR, Liu Z, Owens SE, Wang X, Xue H, Lord A, Kanamarlapudi V, Xia Z. Role of hypoxia inducible factor 1α in cobalt nanoparticle induced cytotoxicity of human THP-1 macrophages. Biomater Transl 2021;2(2):143–50.
[62] Kumanto M, Paukkeri EL, Nieminen R, Moilanen E. Cobalt (II) chloride modifies the phenotype of macrophage activation. Basic Clin Pharmacol Toxicol 2017;121(2): 98–105.
[63] Klopfleisch R. Macrophage reaction against biomaterials in the mouse model - phenotypes, functions and markers. Acta Biomater 2016;43:3–13.